# A Vector Quantization-Based U-Net for Robust Segmentation of Corpus Callosum

Amal JLASSI
*SIIVA, LIMTIC*
*University of Ibn Khaldoun (UIK)*
Tunis, Tunisia
amal.jlassi@uik.ens.tn

Maram ISSAOUI *University of Ibn Khaldoun (UIK)*
TUNISIA
issaouimaram1@gmail.com

Sami HAFSI *LACS ENSTAB*
Tunis, Tunisia
sami.hafsi@enstab.ucar.tn

Ezequiel de la ROSA
*Department of Quantitative Biomedicine University of Zurich*
Zurich, Switzerland
ezequiel.delarosa@uzh.ch

Ahmed HARBAOUI
*Tunis Military Hospital*
Tunis, Tunisia
email address or ORCID

***Abstract*—Automated segmentation of the Corpus Callosum (CC) from brain MRI images is essential for the diagnosis and monitoring of neurological disorders. However, substantial vari- ability in MR intensities across different vendors and protocols, as well as differences in the shape and volume of the CC, pose significant challenges to achieving accurate and reliable segmentation. In this study, we propose an efficient segmentation approach using a novel Vector Quantization-based U-Net (VQ-U-Net). Our architecture builds upon the traditional U-Net model by integrating a Vector Quantization (VQ) memory module within the bottleneck layer. This enhancement enriches feature representation while reducing the model's dependency on large annotated datasets. Additionally, by incorporating saliency map techniques, our model improves interpretability, enabling more trustworthy volumetric quantification of the CC. Experimental results demonstrate that the proposed VQ-UNet significantly outperforms state-of-the-art methods, achieving up to 2% higher Dice scores compared to U-Net variants. We believe this approach paves the way for more reliable CC analysis in clinical settings.**

***Index Terms*—Corpus Callosum, Vector Quantization, U-Net, Segmentation, Grad-CAM**

## I. Introduction

Neurodegenerative diseases affect millions globally and place a heavy burden on healthcare systems. According to the World Health Organization, approximately 47.5 million people are affected, with 7.7 million new cases each year [1]. Conditions such as Alzheimer's disease, epilepsy, and Autism Spectrum Disorder (ASD) are increasingly prevalent [2].

The Corpus Callosum (CC), the brain's largest white matter structure, plays a vital role in connecting the two hemispheres and integrating cognitive, sensory, and motor functions [3]. Abnormalities in CC shape have been associated with disorders such as epilepsy, Alzheimer's, ASD, and psychosis [4], [5]. However, manual inspection of the CC in MRI scans is often unreliable due to inter- and intra-observer variability. Furthermore, its similarity in intensity to nearby structures like the fornix makes precise identification challenging [6].

These difficulties have highlighted the need for automated CC segmentation methods. However, variability in CC shape and intensity, as well as limited annotated data, make this task particularly challenging. Despite promising advances, accurate and robust segmentation remains difficult [8].

To address these issues, we propose a novel Vector Quantization-UNet-based method for CC segmentation with three key improvements:

- Integration of a Vector Quantization (VQ) module in the bottleneck to compress and discretize features, enhancing generalization on limited data.
- A hybrid encoder-decoder with multi-scale convolutional blocks for capturing both local and global context.
- A custom loss function that emphasizes challenging regions, improving segmentation accuracy.

Additionally, we incorporate explainability tools such as Score-CAM [9] and Grad-CAM [10] to support visual interpretation of results, aiding clinical trust and adoption.

## II. Related Work

### A. Deep learning for CC segmentation

CC delineation is a very challenging task because of the need to consider more than just local information, such as edges or region homogeneity. Although clinicians possess a mental image of what the structure should look like—based on prior knowledge of its shape and appearance—accurately segmenting the CC manually requires extensive training and expertise. To address this challenge, various methods have been developed to support the process of CC delineation. In fact, the U-Net model was investigated for CC segmentation

in the study by Chandra et al. [11], incorporating various data augmentation techniques. More recently, a comparative analysis was conducted to evaluate the performance of three distinct deep learning models [12]: CE-Net, U-Net++, and MultiResU-Net. The findings indicated that CE-Net achieved the highest accuracy among the models tested. Furthermore, Chandra et al. [13] introduces a Fully Convolutional Network (FCN) built upon the U-Net architecture, designed specifically for automated CC segmentation from 2D brain MRI images, referred to as CCsNeT. More recently, Padmanabha and Saranya [14] introduced a segmentation model specifically designed for accurate CC segmentation in brain MRIs. This model integrates bidirectional LSTM and Convolutional Block Attention Module (CBAM) classifiers, trained using optimally selected features.

### *B. Incorporating VQ-memory into deep networks*

Recently, vector quantization has been introduced into deep learning for segmentation tasks [15] , improving their efficiency and effectiveness. The purpose of the quantization block is to simplify the latent space by effectively compressing the continuous latent space into a set of discrete vectors by reducing redundant information. The process begins with the definition of a *codebook*, which is a collection of sample vectors that represent the latent conflict space. Data representation process. We define a discrete uniform prior to the codebook vectors as the underlying probability distribution. During training, the model learns a categorical distribution in which each latent embedding is represented by a golden coding vector. This single-shot vector represents the closest codebook vector, effectively quantizing the continuous latent space into discrete units.

Mathematically, the quantization process can be described as follows:

- **Codebook Definition:** Let $\mathcal{C} = \{c_1, c_2, \ldots, c_K\}$ be the codebook consisting of $K$ vectors $c_i \in \mathbb{R}^d$.
- **Embedding Mapping:** For each embedding vector $z \in \mathbb{R}^d$ in the latent space, find the nearest codebook vector $c_k$ such that:

$$k \;=\; \arg\min_i \|z - c_i\|_2 \tag{1}$$

  where $\|\cdot\|_2$ denotes the Euclidean distance.
- **One-Hot Encoding:** Represent the mapping using a one-hot encoded vector $e \in \mathbb{R}^K$ where

$$e_i = \begin{cases} 1, & \text{if } i = k, \\ 0, & \text{otherwise.} \end{cases} \tag{2}$$

- **Discrete Latent Representation:** The quantized representation $\hat{z}$ is then given by:

$$\hat{z} = c_k \tag{3}$$

By combining VQ, the feature benefits from a more compact and structured structure, which leads to better segmentation performance. The quantization technique alleviates overfitting by controlling the instance separation of the latent space, thereby increasing the generalization potential. It also reduces the memory footprint and requirements of the model, making the model more efficient. This method is useful in image segmentation, where accuracy and efficiency are important.

In this paper, we demonstrate performance gains on CC segmentation by integrating the well-known U-Net architecture with a VQ strategy. This integration provides a better and more accurate identification of CC structure, improving its segmentation and possibly its clinical downstream applications.

## III. METHODS

### *A. VQ-Memory*

#### *1) Model architecture :*

- **Embedding Layer**
  The **Vector Quantizer (VQ)** layer transforms the continuous latent space into a discrete representation [16].This is achieved through a codebook

$$\mathbf{E} \in \mathbb{R}^{K \times D},$$

  where $K$ is the number of embeddings and $D$ is the embedding dimension.
  Given an input tensor $z \in \mathbb{R}^{H \times W \times D}$ from the encoder, we flatten it into $z_{\text{flat}} \in \mathbb{R}^{N \times D}$, where $N = H \cdot W$. Quantization is performed by finding the nearest embedding vector $e_k$ in the codebook:

$$k \;=\; \arg\min_j \| z_{\text{dat}} - e_j \|^2 \tag{4}$$

  with

$$j \in \{1, \ldots, K\}.$$

  The quantized output $z_q$ is computed as:

$$z_q \;=\; \text{reshape}\big(\mathbf{E}\,\mathbf{Q},\, \text{shape}(z)\big) \tag{5}$$

  where $\mathbf{Q} \in \{0,1\}^{N \times K}$ is a one-hot encoding matrix indicating the selected embeddings.
  To jointly optimize the codebook and network, the loss $\mathcal{L}_{\text{VQ}}$ is defined as:

$$\mathcal{L}_{\text{VQ}} = \big\|\text{sg}(z_q) - z\big\|^2 + \beta\,\big\|z_q - \text{sg}(z)\big\|^2, \tag{6}$$

  where $\text{sg}(\cdot)$ denotes the stop–gradient operator and $\beta$ is the commitment cost.

- **Encoder**
  The encoder compresses the input $\mathbf{x} \in \mathbb{R}^{H_0 \times W_0 \times C}$ into a latent representation $z \in \mathbb{R}^{H \times W \times D}$ using $L$ convolutional layers and max-pooling. The per-layer formula is:

$$z_l \;=\; \sigma\big(W_l * z_{l-1} + b_l\big), \quad l \in \{1, \ldots, L\}, \tag{7}$$

  where $W_l, b_l$ are the weights and biases of layer $l$, $\sigma$ is ReLU, and $*$ is convolution. Max-pooling reduces spatial dims by 2 at each level:

$$H_{l+1} = \tfrac{H_l}{2}, \quad W_{l+1} = \tfrac{W_l}{2}. \tag{8}$$

The final output of the encoder is z, which is passed to the VQ layer.

- **Vector Quantization (VQ) Memory Layer**
  In the context of corpus callosum segmentation, the Vector Quantization (VQ) layer plays a crucial role in learning discrete latent representations of brain images while preserving the spatial integrity necessary for accurate segmentation. The VQ layer discretizes the continuous latent representations **z** produced by the encoder into a set of embeddings from a learned codebook **E**. This discretization allows the model to effectively capture relevant features while leveraging a finite set of representative codebook vectors, thus reducing the complexity of the latent space. Mathematically, the quantization process in our model can be described as follows:

$$z_q \;=\; \arg\min_{e} \;\| \, z - e\|^2, \quad e \in \mathbf{E}, \tag{9}$$

  where:
  - $z$ represents the continuous latent vector output from the encoder.
  - $z_q$ is the quantized latent vector that gets mapped to the nearest codebook vector $e$.
  - **E** is the codebook of embeddings learned by the VQ layer.

  In the segmentation task, the input images, which contain 3D brain scans with the CC region, are passed through an encoder that learns to map them to a continuous latent space. The VQ layer then discretizes these continuous representations by mapping them to the closest embeddings in the codebook **E**. This allows the model to focus on discrete patterns in the data, improving its ability to learn meaningful features for segmentation.
  The stop-gradient trick is applied during training to ensure differentiability in the optimization pro- cess. Specifically, the quantized representation zq is passed back to the decoder, while the gradient is prevented from flowing through the quantization step. This is achieved by applying the stop-gradient operation.
  Thus, in our case, the VQ layer helps the model learn a compact and discrete representation of the features in the brain images, which are essential for accurate segmentation of the corpus callosum. The encoder maps the input image to a continuous latent space, and the VQ layer discretizes this space, allowing the model to focus on representative patterns while ensuring smooth backpropagation using the stop-gradient trick.
- **Decoder**
  The decoder reconstructs the input $x$ from the quantized representation $z_q$. It uses a combination of upsampling and convolution layers, augmented by skip connections from the encoder:

$$z_{l+1} \;=\; \mathrm{Upsample}(z_l) \;+\; z_{L-l}, \tag{10}$$

  where $\mathrm{Upsample}$ doubles the spatial dimensions, and $z_{L-l}$ are the skip connections from the encoder.

  The final layer applies a convolution with a sigmoid activation to produce the reconstructed image $\hat{x}$:

$$\hat{x} \;=\; \sigma\big(W_{\text{out}} * z_L + b_{\text{out}}\big). \tag{11}$$

- **Vector Quantization (VQ) Loss**
  In the context of a VQ model, the objective is to discretize the continuous latent representations produced by the encoder. The VQ loss encourages the encoder to map the input data to discrete vectors from a predefined codebook, while ensuring that the reconstructions from the decoder are accurate. The VQ loss can be decomposed into two main terms:
  1) **Reconstruction Loss:** This term ensures that the reconstructed image is close to the original image.
  2) **Commitment Loss:** This term prevents the en- coder from drifting too far from the codebook vectors, thus encouraging the encoder's output to align with discrete codebook entries. The VQ loss is defined as follows:

$$\mathcal{L}_{\text{VQ}} = \; \big\|\mathrm{sg}(z_q) - z\big\|^2 \;+\; \beta\,\big\|z_q - \mathrm{sg}(z)\big\|^2 \tag{12}$$

  where:
  - $z$ is the continuous latent vector produced by the encoder,
  - $z_q$ is the quantized version of $z$ (after applying the vector quantizer),
  - $\mathrm{sg}(\cdot)$ denotes the stop-gradient operation (used to prevent backpropagation through the quantization step),
  - $\beta$ is the commitment cost, a hyperparameter that controls the trade-off between the encoder's latent representation and the quantized codebook vectors.

  The VQ loss contains two parts:

  1) **Reconstruction Term:**

$$\big\|\mathrm{sg}(z_q) - z\big\|^2$$

  - This term minimizes the distance between the quantized codebook vector $z_q$ and the continuous encoder output $z$.
  - The stop-gradient operator $\mathrm{sg}(\cdot)$ ensures that this term does not contribute to gradient flow through the quantization process, making it a non-differentiable step.

  2) **Commitment Term:**

$$\big\|z_q - \mathrm{sg}(z)\big\|^2$$

  - This term enforces that the encoder output $z$ is close to the quantized codebook vector $z_q$, preventing large deviations between them.
  - It helps the model avoid having a continuous latent space that is very different from the codebook, improving stability during training.

### B. Commitment Cost ($\beta$)

The commitment cost $\beta$ is a crucial hyperparameter that controls the strength of the commitment loss [17]. When $\beta$ is too small, the encoder can produce latent vectors that deviate significantly from the quantized codebook, resulting in poor representations. If $\beta$ is too large, the latent output of the encoder becomes too close to the codebook vectors, reducing the flexibility of the encoder. Thus, the optimal choice of $\beta$ balances the two terms for effective learning.

### C. Total Loss Function

The total loss function combines the VQ loss with the reconstruction loss, encouraging high-quality reconstructions and stable vector quantization. The total loss function is given by:

$$\mathcal{L}_{\text{total}} = \mathcal{L}_{\text{rec}} \ + \ \mathcal{L}_{\text{VQ}}, \tag{13}$$

where $\mathcal{L}_{\text{rec}}$ is the reconstruction loss, typically computed as the Mean Squared Error (MSE) between the input image $x$ and the reconstructed image $\hat{x}$:

$$\mathcal{L}_{\text{rec}} = \| x - \hat{x} \|^2. \tag{14}$$

Thus, $\mathcal{L}_{\text{total}}$ ensures that the model learns to both reconstruct the input data accurately and quantize the latent space efficiently.

### D. Training Considerations

The VQ loss involves balancing the reconstruction loss and the quantization process. The encoder must learn to output latent representations that are not only informative but also compatible with the codebook. The decoder, in turn, must be able to accurately reconstruct the original input from these quantized latent vectors. The hyperparameter $\beta$ plays a critical role in controlling how much influence the commitment loss has during training, making it a vital part of tuning the model's performance.

## IV. Experiments

### A. Data

We used Sagittal T1-weighted MRI of the brain shows partial agenesis of the corpus callosum from the ABIDE (Autism Brain Imaging Data Exchange) dataset to test the proposed method [18]. The ABIDE dataset is a repository of sagittal brain scans designed to advance biomarker discovery and improve understanding of autism spectrum disorders by collecting and sharing neuroimaging and phenotypic data from multiple sources worldwide. The sagittal scan provides a lateral view of the brain, cropped to the left and right. This perspective provides a detailed view of the central brain. The dataset of 2198 images is split into 70% for training and 30% for testing. This results in 1539 images for training and 659 images for validation.This dataset is composed of two large-scale collections called ABIDE-I and ABIDE-II. It is worthy noting that we have a challenging heterogeneous set of images of normal subjects and individuals with Autism.

### B. Implementation details

We implemented our model using TensorFlow and Keras, incorporating a U-Net architecture enhanced with VQ for semantic segmentation tasks. The model architecture includes multiple convolutional layers for encoding and decoding, with each layer optimized to capture hierar- chical features. The VectorQuantizer layer within the network utilizes a specified number of embeddings and embedding dimensions, controlled by a commitment cost parameter to facilitate efficient clustering of input data. We initialized the model with an input shape of (256, 256, 1) and trained it using Adam optimizer with a binary cross-entropy loss function. Throughout training, we monitored metrics such as accuracy, Jaccard Index, recall, and Dice coefficient to evaluate segmentation performance on both training and validation datasets.

### C. Comparison with other state-of-the-art models

In this section, we compare our model with state-of-the-art methods including UNet++ [12], CE-Net [12], MultiResUNet [12], CCSNeT [13], and Optimized UNet [14]. As shown in Table I, our method outperforms others in most metrics, achieving a Dice Coefficient of 99.81% and Accuracy of 99.58%. While Optimized UNet shows slightly higher sensitivity, our model delivers more balanced and accurate segmentation overall.

TABLE I
COMPARISON WITH OTHER MODELS. THE BEST RESULTS ARE HIGHLIGHTED IN BOLD.

| **Models** | **Metrics (%)** | | |
|---|---|---|---|
| | **Dice Coefficient** | **Accuracy** | **Specificity** |
| UNet++ [12] | 71.68 | 99.36 | 99.44 |
| CE-Net [12] | 93.11 | 99.89 | 99.94 |
| MultiResUNet [12] | 80.20 | 79.71 | 79.55 |
| CCSNeT [13] | 96.74 | – | – |
| Optimized UNet [14] | 97.81 | 96.28 | **98.83** |
| **Proposed Method** | **99.81** | **99.58** | 94.90 |

Although our model may show a slightly higher false negative rate, this is likely due to architectural or training differences that prioritize overall segmentation quality over sensitivity.

In our proposed method, both Grad-CAM and Score-CAM are employed to visualize and interpret the model's decision-making process. Grad-CAM generates heatmaps using gradients to highlight important regions in the input image, providing a broad view of where the model fo- cuses during segmentation. In contrast, Score-CAM leverages the model's confidence scores to produce clearer and more precise localization of features, particularly isolating the CC region with sharper boundaries. These complementary visualization techniques not only confirm that our model accurately captures the relevant anatomical features but also offer critical insights for further refinement, ultimately enhancing segmentation performance and clinical applicability.

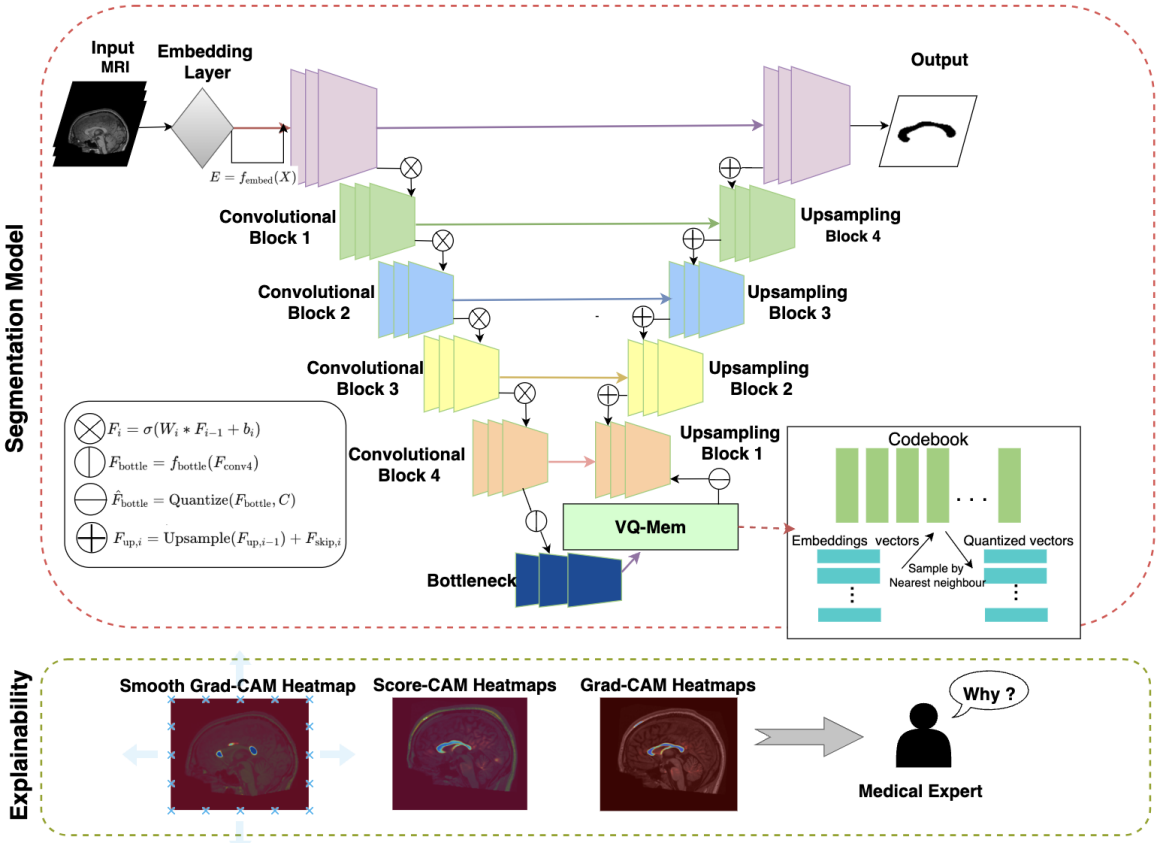


Fig. 1. Proposed model. Top: VQ-U-Net architecture. Bottom: Explainability analysis.

Fig. 2 illustrates qualitative results on the ABIDE dataset. According to our clinical collaborator, the segmented CC accurately represents its anatomical subdivisions—especially the rostrum and splenium—while effectively excluding the fornix. The CC masks provide clear and precise delineation without including irrelevant nearby structures.

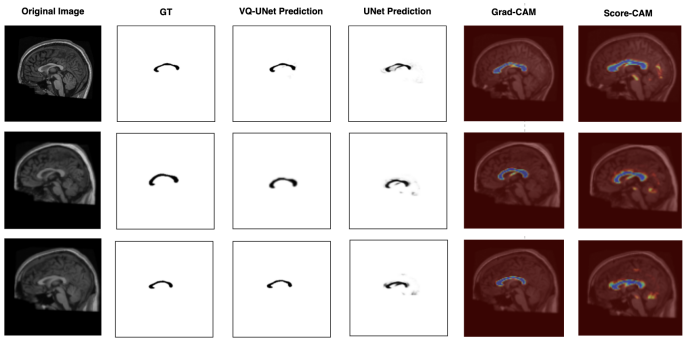


Fig. 2. Comparison of segmentation performance across different models and visualization techniques. First column: Original MRI images. Second column: Ground truth (GT) segmentation of the CC. Third column: Predictions from the proposed VQ-UNet model. Fourth column: Predictions from the standard UNet model. Fifth column: Grad-CAM visualization highlighting important regions influencing the model's decision. Sixth column: Score-CAM visualization providing an alternative attention-based explanation of model predictions.

**Ablation Study :**

As shown in Table II, ablation experiments were conducted to assess the impact of integrating the VQ memory mechanism into the U-Net architecture. Starting from a baseline U-Net model, we observed performance improvements with the addition of VQ and data augmentation.

The baseline U-Net, without augmentation or VQ, achieved a Dice Coefficient of 87.9% and a loss of 50.9%. Adding data augmentation alone slightly improved performance to 89.2%, with a loss of 87.87%. In contrast, incorporating VQ significantly boosted the Dice Coefficient to 99.6% and reduced the loss to 8.2%. The best results were obtained when both augmentation and VQ were applied, reaching a Dice Coefficient of 99.8% and a minimal loss of 1.7%. These results confirm the complementary effect of VQ and augmentation in enhancing segmentation accuracy and reducing errors.

## V. DISCUSSION

**Deep Learning Versus Experts: Qualitative analysis**

To evaluate the performance of our UNet-VQ model, we collaborated with neurosurgeons at a military hospital in Tunisia. A blind evaluation was conducted on 60 segmented images, with 52 correctly segmented, yielding a success rate of 86.67%. As shown in Fig.3, which presents the interquartile range (IQR), median values, and outliers, the model demonstrated consistent and reliable results. The compact IQR and

TABLE II
ABLATION STUDY OF OUR MODEL

| U-Net Baseline | Data augmentation | VQ | Metrics | |
|---|---|---|---|---|
| | | | Dice Coefficient | Validation Loss |
| ✓ | × | × | 87.9% | 50.9% |
| ✓ | ✓ | × | 89.2% | 87.87% |
| ✓ | × | ✓ | 99.6% | 8.2% |
| ✓ | ✓ | ✓ | 99.8% | 1.7% |

median scores between 7 and 7.5 out of 10 confirm stable performance across cases.

Although 13.33% of the segmentations were rated inadequate, the consistent nature of these errors offers insights for improvement in edge and complex cases. Experts also reported difficulty distinguishing between original and segmented images, suggesting human-level accuracy in standard scenarios. Despite these promising outcomes, limitations such as the single-center setup and small dataset highlight the need for broader validation. Future work will involve multicenter studies and improved quality assurance for enhanced clinical applicability.

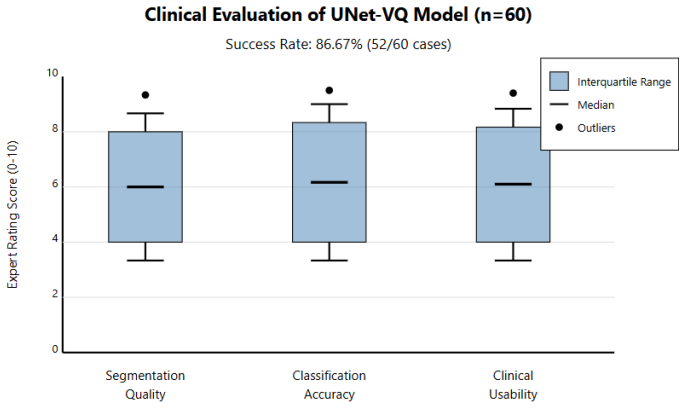


Fig. 3. Analysis of UNet-VQ Model Performance in Clinical Evaluation

## VI. CONCLUSION

In this paper, we presented a novel Vector Quantization based U-Net method for the automatic CC segmentation within MRI images. Three key enhancements were introduced: the integration of a Vector Quantization module within the bottleneck layer to improve feature representation, the use of a hybrid encoder-decoder architecture optimized for multi-scale feature extraction, and a custom loss function to enhance segmentation in challenging regions. These contibutions resulted in superior performance across metrics such as the Dice coefficient, Jaccard index, and recall, outperforming other state of the art methods and demonstrating the potential for robust clinical applications.

## REFERENCES


[1] A. Lohani, M. Maurya, R. Kaur, A. Gaur, S. Khan, and N. Verma, "Nutraceutical's Potentials in Neurodegenerative Disease," Nutraceutical Fruits and Foods for Neurodegenerative Disorders, Academic Press, vol. 1, no. 1, pp. 199–213, 2024.

[2] D. A. M. Kamal, S. Z. Abidin, W. S. W. Saudi, J. Kumar, and A. Bellato, "Roles of Prostaglandins and Cyclooxygenases in Autism Spectrum Disorder: A Comprehensive Review," Current Behavioral Neuroscience Reports, vol. 12, no. 1, pp. 1–15, 2025.

[3] A. Jlassi, K. ElBedoui, and W. Barhoumi, "ACCP-MC-U-Net: Automatic Corpus Callosum Parcellation from brain MRI scans using MultiClass U-Net," in Proc. 2023 Int. Conf. on Innovations in Intelligent Systems and Applications (INISTA), Sep. 2023, pp. 1–6, IEEE.

[4] T. Sevimoglu, T. Bal, and Ç. Özdemir, "Brain Diseases and Disorders," Bioinformatics of the Brain, CRC Press, vol. 1, no. 1, pp. 1–41, 2024.

[5] A. Jlassi, K. Elbedoui, W. Barhoumi, and C. Maktouf, "3DCC-MPNN: Automated 3D reconstruction of corpus callosum based on modified PNN and marching cubes," Evolving Systems, vol. 1, no. 1, pp. 1–27, 2024.

[6] A. Jlassi, K. ElBedoui, W. Barhoumi, and C. Maktouf, "Unsupervised Method based on Probabilistic Neural Network for the Segmentation of Corpus Callosum in MRI Scans," in VISIGRAPP (4: VISAPP), vol. 1, no. 1, pp. 545–552, 2019.

[7] N. Siddique, S. Paheding, C. P. Elkin, and V. Devabhaktuni, "U-Net and its variants for medical image segmentation: A review of theory and applications," IEEE Access, vol. 9, no. 1, pp. 82031–82057, 2021.

[8] M. Platten, I. Brusini, O. Andersson, R. Ouellette, F. Piehl, C. Wang, and T. Granberg, "Deep learning corpus callosum segmentation as a neurodegenerative marker in multiple sclerosis," Journal of Neuroimaging, vol. 31, no. 3, pp. 493–500, 2021.

[9] Y. Brima and M. Atemkeng, "Saliency-driven explainable deep learning in medical imaging: bridging visual explainability and statistical quantitative analysis," BioData Mining, vol. 17, no. 1, pp. 1–33, 2024.

[10] K. Raghavan, "Attention guided grad-CAM: an improved explainable artificial intelligence model for infrared breast cancer detection," Multimedia Tools and Applications, vol. 83, no. 19, pp. 57551–57578, 2024.

[11] A. Chandra, S. Verma, A. S. Raghuvanshi, N. D. Londhe, N. K. Bodhey, and K. Subham, "Corpus callosum segmentation from brain MRI and its possible application in detection of diseases," in 2019 IEEE Int. Conf. on Electrical, Computer and Communication Technologies (ICECCT), vol. 1, no. 1, 2019.

[12] S. Shrivastava, N. Singh, U. Mishra, A. Chandra, and S. Verma, "Comparative study of deep learning models for segmentation of corpus callosum," in 2020 4th Int. Conf. on Computing Methodologies and Communication (ICCMC), vol. 1, no. 1, 2020.

[13] A. Chandra, S. Verma, A. S. Raghuvanshi, and N. K. Bodhey, "CCsNeT: Automated corpus callosum segmentation using fully convolutional network based on U-Net," Biocybernetics and Biomedical Engineering, vol. 42, no. 1, pp. 187–203, 2022.

[14] S. A. Padmanabha and G. Saranya, "Segmentation of the corpus callosum from brain magnetic resonance images using dual deep learning classifiers and optimized U-shaped neural networks," SN Comput. Sci., vol. 5, no. 1, pp. 1–10, 2023.

[15] S. Huang, T. Xu, N. Shen, F. Mu, and J. Li, "Rethinking few-shot medical segmentation: a vector quantization view," in Proc. IEEE/CVF Conf. on Computer Vision and Pattern Recognition (CVPR), vol. 1, no. 1, pp. 3072–3081, 2023.

[16] Y. Zhang, D. S. Carvalho, M. Valentino, I. Pratt-Hartmann, and A. Freitas, "Improving semantic control in discrete latent spaces with transformer quantized variational autoencoders," arXiv preprint arXiv:2402.00723, vol. 1, no. 1, pp. 1–10, 2024.

[17] T. Seghair, O. Besbes, T. Abdellatif, and S. Bihiri, "VQ-VGAE: Vector Quantized Variational Graph Auto-Encoder for Unsupervised Anomaly Detection," in 2024 IEEE Int. Conf. on Big Data (BigData), vol. 1, no. 1, pp. 2370–2375, 2024.

[18] A. Ashraf, Q. Z., W. H. K. Bangyal, and M. Iqbal, "Analysis of brain imaging data for the detection of early age autism spectrum disorder using transfer learning approaches for internet of things," IEEE Trans. on Consumer Electronics, vol. 70, no. 1, pp. 4478–4489, 2023.